Int. J. Electrochem. Sci., 14 **(2019)** 1 – 14, doi: 10.20964/2019.01.50

International Journal of
ELECTROCHEMICAL
SCIENCE
www.electrochemsci.org

Porous Carbon Material based on Biomass Prepared by MgO Template Method and $ZnCl_2$ Activation Method as Electrode for High Performance Supercapacitor

Qingyang Sun[1], *Tianyao Jiang* [1], *Guangzhen Zhao and Junyou Shi*[1,2,*]

[1] Northeastern Electric Power University, College of Chemical Engineering, Jilin 132012, China
[2] Beihua University, Forestry College, Jilin 132013, China
[*]E-mail: bhsjy64@163.com

Received: 4 September 2018 / *Accepted:* 1 November 2018 / *Published:* 30 November 2018

Here, we use cotton as a biomass material, MgO as a templating agent, and $ZnCl_2$ as an activator to prepare a biomass-based porous carbon material. As a pore generator, MgO is incorporated into cotton carbon by absorbing a solution of $Mg(NO_3)_2$ in cellulose fibers, subsequent drying and carbonization processes. After removing the MgO template by acid leaching, a biomass-based porous carbon material having a low cost and a high specific surface area is prepared. $ZnCl_2$ has the functions of dehydroxylation and dehydration during the activation process, so that hydrogen and oxygen in the raw material are released in the form of water vapor to form a porous structure. Moreover, $ZnCl_2$ is transferred to ZnO during the activating process. The ZnO particles in the obtained material are removed by acid washing, and then these remained voids contribute additional porosity in internal structure. The experimental results show that the activated carbon material prepared by using MgO as the template agent $ZnCl_2$ as the activator has a specific surface area of up to 1990 $m^2 g^{-1}$. In the three-electrode system test, the current density is 1 A g^{-1} and the capacitance is 240 F g^{-1}. When the current density is 20 A g^{-1}, the specific capacitance is 173 F g^{-1}, and the capacitance retention rate is 71%. In addition, the assembled symmetric supercapacitors were tested in 6M KOH aqueous solution and 1M Na_2SO_4 aqueous solution, respectively. The energy density in the alkaline system is 5.7 Wh kg^{-1}. The energy density in the neutral electrolyte is 12.5 Wh kg^{-1} and the cycle stability is 89%.

Keywords: Biomass-based porous carbon, MgO template method, $ZnCl_2$ activation method, supercapacitor

1. INTRODUCTION

Nowadays, due to over-exploitation of fossil energy, energy shortage and environmental degradation, energy storage devices are needed to reduce the consumption of natural energy [1]. Supercapacitor is a form of green high-efficiency energy storage device, which is widely used in high-power energy storage systems such as hybrid electric vehicles and load balancing equipment [2].

Compared with other energy storage devices, it has the advantages of high power density, fast charge and discharge speed, and high cycle stability [3]. Electrode materials are an important part of supercapacitors, mainly including carbon materials [4], metal oxides [5], conductive polymers [6], conductive polymers and mental oxides have been used to increase the specific capacitance via a variety of reversible oxidation states for highly efficient redox charge transfer [7]. But the practical application of the pseudocapacitive material is constrained by its high price, instability of circulation and low electrical conductivity [8]. In contrast, carbon materials have the advantages of excellent electrical properties, good cycle stability, and high specific surface area, and are therefore one of the most commonly used electrode materials [9]. Carbon electrode materials include activated carbon [10], carbon fiber [11], and carbon nanotubes [12]. Among them, activated carbon materials have become the main material for the fabrication of supercapacitor storage electrodes due to their low-cost production process [13]. Precursors for the preparation of carbon materials are quite extensive, such as coal [14], but due to the shortage of fossil energy, a low-cost and sustainable raw material is needed as a precursor [15]. Therefore, the development of biomass as a precursor of carbon materials with structurally controllable high-performance carbon materials has received extensive attention [16].

So far, scholars have carried on an extensive research of carbon materials in nature, a potential electrode materials for supercapacitors. Lotus stems [17], wild rice stem [18], fungus [19], and cotonier strobili [20] are regarded as potential precursors for the synthesis of activated carbons. It is well known that Cotton, one of the most significant agricultural commodities, is cultivated and produced widely [21]. Cellulose is a major component of cotton. Cellulose contains a large amount of carbon and is sintered at high temperature to carbon under nitrogen protection [22, 23]. The addition of a template agent during the carbon burning process can make the arrangement of the pores of the carbon material more orderly, increase the number of pores, increase the specific surface area of the carbon material, and thereby cause accelerate the rate of movement of anions and cations from the positive to the negative electrodes in the electrolyte [24]. Thereby improving the electrochemical performance. The addition of an activator can increase the number of pores of the carbon material, and the increase in the number of pores can also cause the migration of anions and cations to both electrodes more quickly, increase the charge transfer rate, and thus have better conductivity [25, 26].

At present, Chunyu Zhu, used cotton to prepare a porous carbon material with a specific surface area of 1260 m^2 g^{-1} by using the MgO template method and applied it to a lithium ion battery [27]. In this paper, cotton fiber is used as carbon source, MgO is used as template and $ZnCl_2$ is used as activator. Cotton-based porous activated carbon is prepared by simple chemical activation one-step method. For comparison, the dried absorbent cotton was directly carbonized and the material immersed only in the $ZnCl_2$ solution and only immersed in $Mg(NO_3)_2$ was carbonized and comparatively analyzed.

2. EXPERIMENTAL

2.1 Preparation of activated carbon materials

Taking the absorbent cotton in the laboratory as raw material, weighing a certain amount of absorbent cotton and immerse it in distilled water for a period of time, filtering it and drying it at 60°C for 5 h. 15 mmol of $Mg(NO_3)_2$ and 4.5 g of $ZnCl_2$ were dissolved in 10 mL of deionized water, 1.5 g of

dried absorbent cotton was dipped into target solution. The cotton completely absorbed the solution, and dry the sample in vacuum space for 24 h and heated it for 2h in a tube furnace of N_2 at 800°C. After it is cooled down to room temperature, grind black sample into powder and wash it with a large amount of dilute hydrochloric acid to remove residual impurities, washed several times with deionized water, and finally dried at 80°C for 12 h. For comparison, the dried absorbent cotton was directly carbonized or the material immersed only in the $ZnCl_2$ solution and only immersed in $Mg(NO_3)_2$ was carbonized and comparatively analyzed.

2.2 Physical performance test

The degree of graphitization of the material was tested by X-ray diffraction (X'Pert Pro, PANalytical BV) and Raman spectroscopy (Renishaw). A scanning electron microscope (S3400N-I, *Hitachi Limite*) was used to characterize the microstructure of the sample. The Brunauer-Emmett-Teller (BET) surface area (S_{BET}) of the samples were analyzed by nitrogen adsorption in a Micromeritics ASAP 2020 nitrogen adsorption apparatus (U.S.A.).

2.3 Electrochemical performance analysis

All electrochemical performance were performed at room temperature using the CHI660E electrochemical workstation. Electrochemical measurements were performed in a three-electrode and two-electrode system, respectively. A mixture of the active material, carbon black and polytetrafluoroethylene (PTFE) binder in a mass ratio of 75:15:10 was coated on foamed nickel (having a size of about $1cm^2$) and dried at 100°C. The material was kept in a vacuum oven for 10 hours at 90 °C. It was nearly 2 mg cm^{-2} that the loading mass of the electrode. In the syetem of three-electrode, take the samples prepared as working electrode and platinum gauze electrode respectively. The Hg / HgO electrode worked as counter and reference electrodes. Make a test of the cyclic voltammetry (CV), constant current charge/discharge and electrochemical impedance spectroscopy (EIS) in a 6 M solution of KOH. Assembling a symmetrical two-electrode supercapacitor using two electrodes of identical mass. Electrochemical measurements were carried out in aqueous solutions of 6 M KOH and 1 M Na_2SO_4, respectively, with potential windows of 0-1 V and 0-1.6 V, respectively.

A calculation of the specific capacitance of the electrode can be got through the charge/discharge curve:

$$C_{SP}=I\Delta t / m\Delta V$$

C_{SP} (F g^{-1}) is the specific capacitance of the supercapacitor mass; I (A) is a constant charge / discharge current density; Δt (s) is the charging time; ΔV (V) is the charging voltage; m (g) is the mass of the active material of the electrode.

The energy density (E) and power density (P) were calculated based on the following equations:

$$E=CV^2 / 2$$

$$P=E /\Delta t$$

C (F g^{-1}) represents the specific capacitance of a symmetric supercapacitor. V (V) represents the discharge voltage. Δt (s) represents the discharge time, E (Wh kg^{-1}) represents the energy density and P (W kg^{-1}) represents the power density.

3. RESULTS AND DISCUSSION

3.1 X-ray diffraction and Roman spectroscopy

X-ray diffraction and Raman spectroscopy are commonly used test methods for studying the degree of graphitization of materials Fig. 1(a) shows that the apparent diffuse diffraction peaks of all carbon materials near the 22.5° diffraction angle are caused by the disordered microcrystalline surface (002), indicating the presence of a large number of amorphous structures in the base carbon compound. A weak diffraction peak near the 45° angle is caused by the (100) crystal plane, indicating the presence of a small amount of graphitized crystal plane in the base carbon compound.

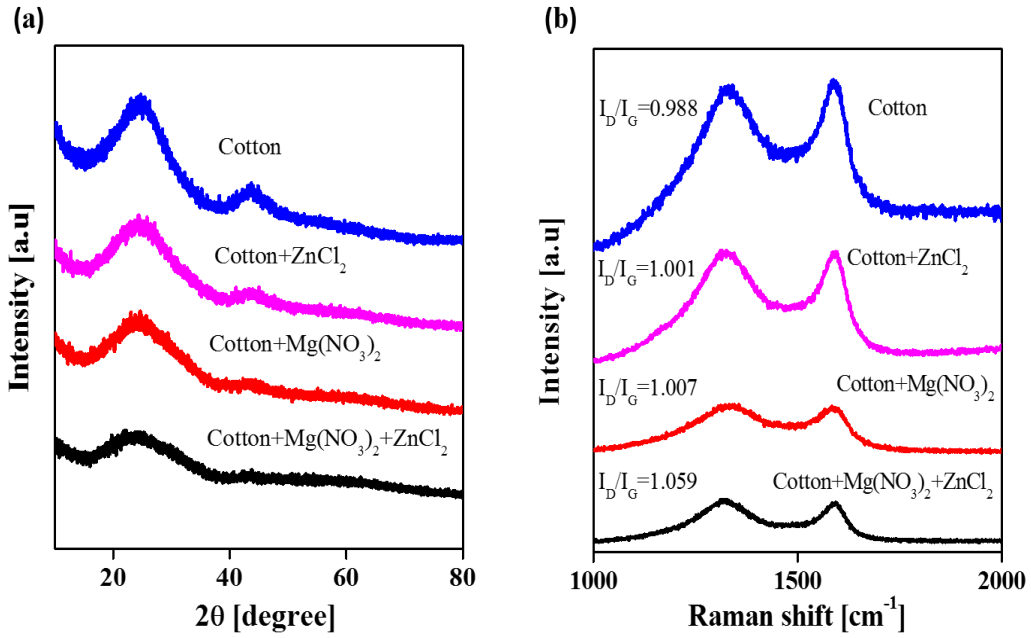

Figure 1. XRD patterns (a) and Raman spectra (b) of the synthesized samples.

Compared with other materials, the carbonized material impregnated in $ZnCl_2$ and $Mg(NO_3)_2$ at the (002) peak broadens and the strength weakens, indicating that the interlayer spacing becomes large and there is chaotic carbon. The reason for this phenomenon is $Mg(NO_3)_2$ will generate MgO during heat treatment. The generated MgO is used as a template agent as a pore generating agent. After removal with acid, a porous structure is formed [27]. As an activator, $ZnCl_2$ has the functions of dehydroxylation and dehydration, so that hydrogen and oxygen in the raw material are released in the form of water vapor in the process of high temperature to form a porous structure, thereby increasing the disorder of the material [28]. Fig. 1(b) is a Raman spectrum and the two peaks correspond to G (1350 cm^{-1}) and D (1586

cm^{-1}), respectively. The intensity ratio of D and G peaks is often used as an important indicator of the proportion of the amorphous content. The ratio of the material ID/IG of the carbonized cotton immersed in $ZnCl_2$ and $Mg(NO_3)_2$ is the largest, indicating that the material has the highest amorphous content. From the above discussion, the conclusion can be arrived that high amorphous content leads to good conduction which was in line with the conclusion drawn from the XRD patterns.

3.2 SEM analysis

In order to see the shape of the material more clearly. Fig. 2(a) shows a carbon material prepared by direct carbonization of absorbent cotton, having a highly twisted rod-like structure on the surface and a slight wrinkle on the surface without significant pores. Fig. 2(b) shows the carbonization of absorbent cotton immersed in $ZnCl_2$, and the surface morphology of the carbon sample changes, showing a small pore structure. Fig. 2(c) shows the pore structure caused by the accumulated wrinkles when the $Mg(NO_3)_2$ treatment is added. Fig. 2(d) shows the carbonization of absorbent cotton impregnated in $ZnCl_2$ and $Mg(NO_3)_2$ solutions. The Figure shows a rich pore structure and a porous structure formed by a large number of pleats, so that the number of pores is improved. The abundant pore structure contributes to the accumulation of charge and the adsorption and transport of electrolyte ions [29-31], which in turn improves the electrochemical performance of the material. These results indicate that $ZnCl_2$ and $Mg(NO_3)_2$ are two vital roles in the process of forming a porous structure during carbonization.

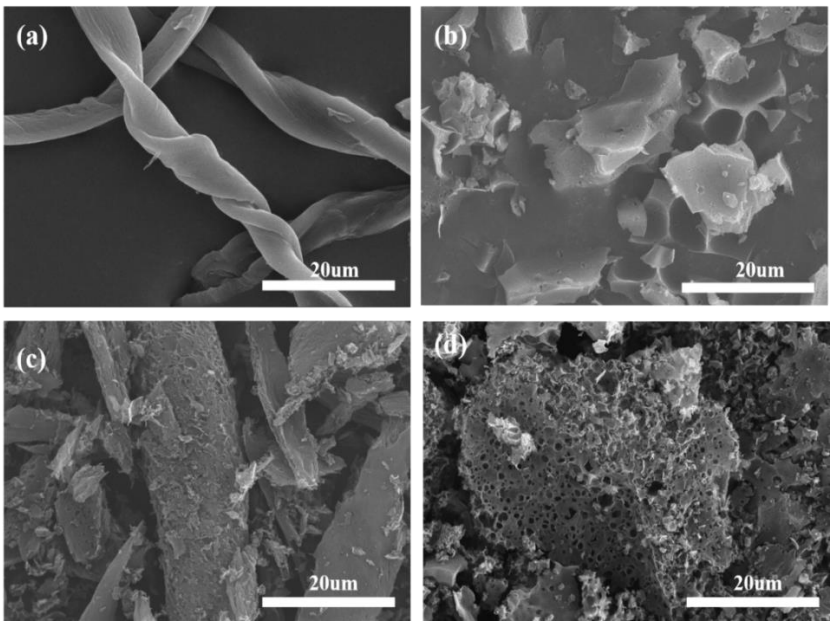

Figure 2. (a) Scanning electron micrograph of direct carbonization of absorbent cotton; (b) Scanning electron micrograph of carbonization of absorbent cotton immersed in $ZnCl_2$; (c) Scanning electron micrograph of carbonization of absorbent cotton immersed in $Mg(NO_3)_2$; (d) Scanning electron micrograph of carbonization of absorbent cotton impregnated in $ZnCl_2$ and $Mg(NO_3)_2$.

3.3 Porosity analysis

To further evaluate the pore properties of in order to evaluate the pore structure of different materials, nitrogen absorption–desorption isothermal analysis were employed. Nitrogen adsorption-desorption isotherms of carbonized materials impregnated with $ZnCl_2$ and $Mg(NO_3)_2$ as shown in the black square line in Fig.3 (a), Presented as type IV. A hysteresis loop exists in the range between 0.40-0.99P / P0 relative pressure. This indicates that the material has a mesoporous structure [32]. Meanwhile, at low relative pressure (P / P0 < 0.40), the adsorption isotherm is rapidly saturated, indicating that it has a microporous structure [33]. The pore size distributions were estimated according to the density functional theory (DFT) method.Fig.3b shows the pore size distribution curves of different materials. It can be seen that the absorbent cotton carbonized material immersed in $ZnCl_2$ and $Mg(NO_3)_2$ has a small amount of micropores and a large number of mesopores. As we all know that the micropores were beneficial the to charges accumulation while mesopores were helpful to the adsorption and transport of electrolyte ions [34-36]. Table1 shows the pore structure parameters of different samples. Compared with other materials, the specific surface area and total pore volume of the carbonized material of the absorbent cotton immersed in $ZnCl_2$ and $Mg(NO_3)_2$ were 1990 m^2g^{-1} and 1.23 $cm^3 g^{-1}$, respectively. The high specific surface area and high pore volume of the material facilitate ion transfer and charge storage of the supercapacitor.

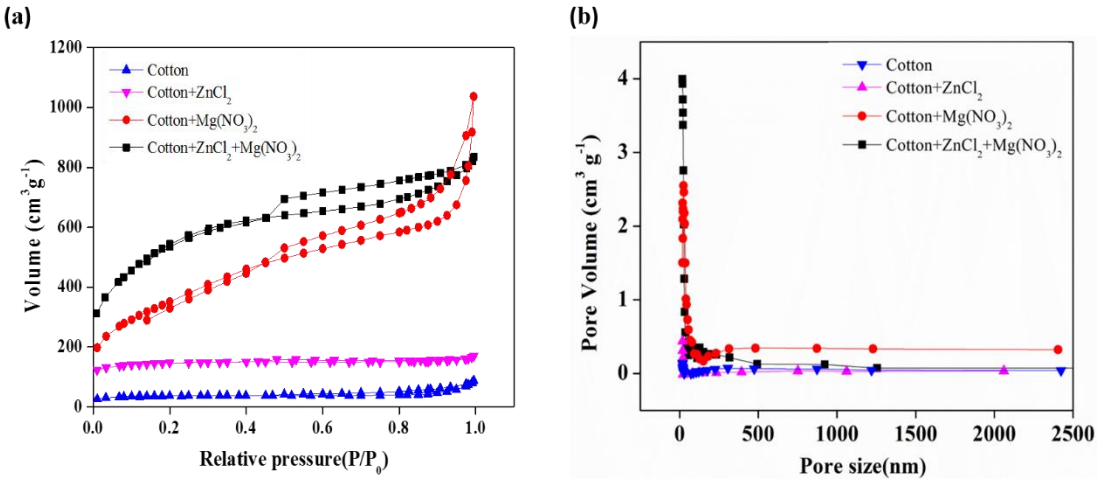

Figure 3. (a) Nitrogen adsorption desorption isotherms of different materials (b) The pore size distribution of different materials

Table 1. The Pore structure parameters of the samples.

Samples	S_{BET}[a] (m^2 g^{-1})	S_{micro}[a] (cm^3 g^{-1})	Pore volume[b] (cm^3 g^{-1})
Cotton	127	80	0.1
Cotton+$ZnCl_2$	663	569	0.34
Cotton+$Mg(NO_3)_2$	1288	30	0.98
Cotton+$ZnCl_2$+$Mg(NO_3)_2$	1990	128	1.23

[a]Specific surface area from multiple BET method

[b]Total pore volume at P/P_0=0.99

3.4 Electrochemical performance analysis

3.4.1 Analysis of electrochemical performance under three-electrode system

Fig.4 is tested under a three-electrode system. The electrolyte is a KOH solution. The materials are direct carbonization of absorbent cotton, carbonization of absorbent cotton immersed in $ZnCl_2$, carbonization of absorbent cotton immersed in $Mg(NO_3)_2$, carbonization of absorbent cotton immersed in $ZnCl_2$ and $Mg(NO_3)_2$. Fig. 4(a) demonstrates the CV curves of different materials (at a scan rate of 100 mV s^{-1}). In the comparison with other materials, the CV curve of the absorbent cotton carbonized material immersed in $ZnCl_2$ and $Mg(NO_3)_2$ is more rectangular and the enclosed area is larger, resulting in a larger specific capacitance. Therefore, the material has a faster charge transfer rate and better electrochemical performance. Fig. 4(b) shows the charge-discharge curves of different electrode materials at a current density of 1 A g^{-1}. It can be seen from the Figure that the charge-discharge curve maintains basic symmetry. Compared with other materials, the electrode material immersed in absorbent cotton in $ZnCl_2$ and $Mg(NO_3)_2$ has a longer discharge time. As a supercapacitor electrode material, the performance is better than other materials. In addition to the fast charge transfer rate of the material, the rate of electromigration, diffusion, and mass transfer of the particles in the electrolyte also increases, demonstrating the reason for this phenomenon due to the porous structure of the material and the high specific surface area. Fig. 4(c) shows CV curves of the electrode material of carbonized absorbent cotton immersed in $ZnCl_2$ and $Mg(NO_3)_2$ at scan rates of 10 mV s^{-1}, 20 mV s^{-1}, 50 mV s^{-1}, 100 mV s^{-1}, 200 mV s^{-1}, and 500 mV s^{-1}. This material exhibits the highest specific capacitance. The phenomenon that the rectangular shape still remained even at the scan rate of 500 mV s^{-1} gives an evidence to the conclusion that the transport and diffusion of charge and electrolyte ion are quick among the samples of electrode.

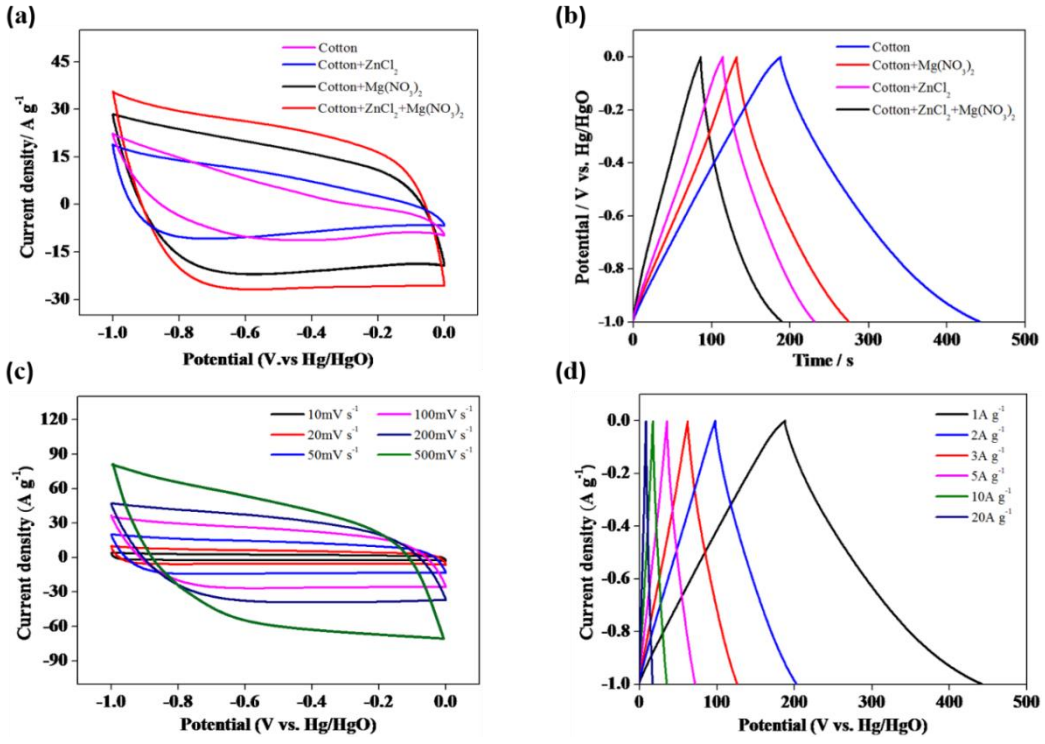

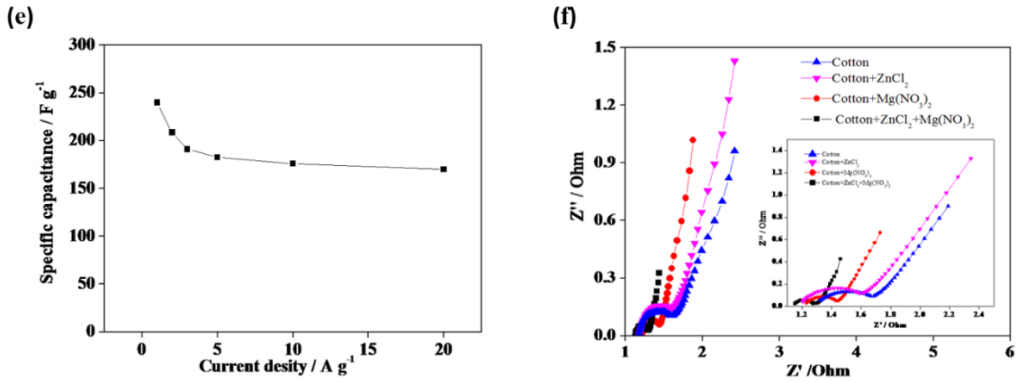

Figure 4. (a) Cycle voltammetry (CV) curves of different materials at a scan rate of 100 mV s^{-1}. (b) Charge and discharge curves of different electrode materials at a current density of 1 A g^{-1}. (c) is an electrode material for carbonization of absorbent cotton immersed in $ZnCl_2$ and $Mg(NO_3)_2$ at scan rates of 10 mV s^{-1}, 20 mV s^{-1}, 50 mV s^{-1}, 100 mV s^{-1}, 200 mV s^{-1}, 500 mV s^{-1} Cyclic voltammetry curve.(d) Electrode materials immersed in absorbent cotton in $ZnCl_2$ and $Mg(NO_3)_2$ at current densities of 1 A g^{-1}, 2 A g^{-1}, 3 A g^{-1}, 5 A g^{-1}, 10 A g^{-1},20 A g^{-1} Charge and discharge curve. (e) The value of the specific capacitance of the electrode material immersed in absorbent cotton in $ZnCl_2$ and $Mg(NO_3)_2$ at different current densities. (f) Electrochemical impedance spectroscopy (EIS) of different electrode materials.

The reason for this phenomenon may be caused by the synergistic effect of the porosity and electrode/electrolyte wettability due to the atoms attached to the surface of porous carbon [37-39]. Fig. 4(d) charge-discharge curves of the electrode material of the carbonized absorbent cotton immersed in $ZnCl_2$ and $Mg(NO_3)_2$ at current densities of 1 A g^{-1}, 2 A g^{-1}, 3 A g^{-1}, 5 A g^{-1}, 10 A g^{-1}, 20 A g^{-1}. The shape of the charge and discharge curve is triangular at different current densities and all curves have good symmetry at different current densities. This means that the material has good capacitance and electrochemical reversibility. Fig. 4(e) is the specific capacitance of the electrode material of carbonized in $ZnCl_2$ and $Mg(NO_3)_2$ at different current densities, it can be seen that the specific capacitance at a current density of 1 A g^{-1} is 240 F g^{-1}, the specific capacitance at a current density of 20 A g^{-1} is 173 F g^{-1}, and the capacitance retention rate is 71%, indicating that the material has good capacitance retention. Fig. 4(f) is an EIS curve for different electrode materials. The kinetic behavior of ion and electron transport was investigated by EIS measurements. The kinetic behavior of ion and electron transport was investigated by EIS measurements [40]. The Nyquist diagram is divided into three areas, including high frequency, intermediate frequency and low frequency curve segments. A semicircle with a smaller diameter means a lower charge transfer resistance [41]. In addition, The intersection of the semicircle and the abscissa reflects the equivalent series internal resistance. [28]. As shown in Fig. 4(f) the electrode material carbonized by defatted cotton in $ZnCl_2$ and $Mg(NO_3)_2$ has the smallest semicircular diameter due to low charge transmission resistance and has the maximum inclination at low frequencies. These values indicate that the material has lower ion mobility and ideal capacitor behavior than other electrode materials. The results may be due to the high specific surface area of the material and a certain degree of graphitization and increased material disorder.

3.4.2 Supercapacitor assembly and performance testing

Figure 5 is an electrochemical test of an assembled symmetric supercapacitor in a KOH electrolyte solution with a potential window of 0-1V. However, in order to expand the potential window and allow the material to have better electrochemical performance in the assembled supercapacitor, a symmetric supercapacitor was tested under a neutral electrolyte. Figure 6 shows the electrochemical test of an assembled symmetric supercapacitor in a Na_2SO_4 electrolyte solution with a potential window of 0-1.6V. The reason why the neutral electrolyte can enlarge the potential window is that the alkali metal sulfate aqueous solution has a balanced hydrogen ion, a strong solvent ratio of the hydroxide ion and the alkali metal cation to the sulfate anion, and the decomposition voltage is higher than the water pressure [28, 42].

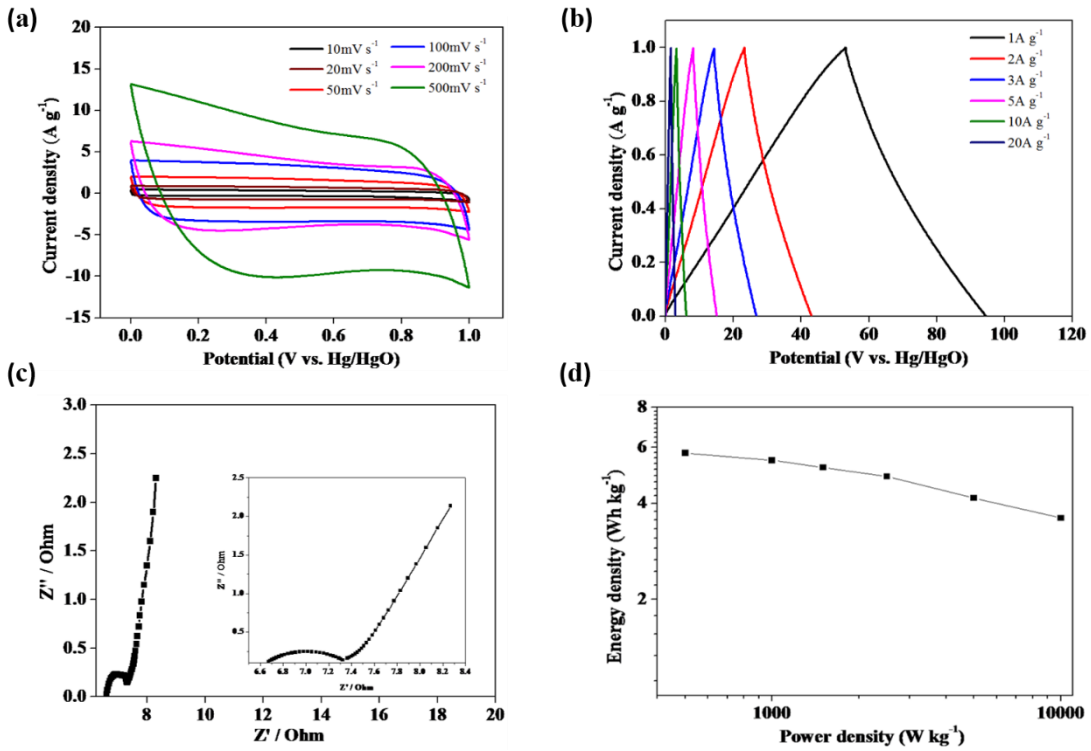

Figure 5. (a) CV curves of different scanning rates with a potential window of 1 V; (b) The current density is a charge-discharge curve of 1 A g^{-1}, 2 A g^{-1}, 3 A g^{-1}, 5 A g^{-1} , 10 A g^{-1} ,and 20 A g^{-1}; (c) EIS curve; (d) The energy density and power density curves of current densities of 1 A g^{-1}, 2 A g^{-1} , 3 A g^{-1} , 5 A g^{-1} , 10 A g^{-1} , and 20 A g^{-1}

In order to evaluate the practical application of electrode materials immersed in absorbent cotton in $ZnCl_2$ and $Mg(NO_3)_2$, we assembled and studied symmetric supercapacitors in 6 M KOH aqueous solution. Fig. 5(a) shows the CV curve at different scan rates for the potential window at 0-1V. All CV curves exhibit an approximately rectangular shape at different scan rates, which means good rate performance and double layer capacitance effects. The reason for this phenomenon is due to the high specific surface area of the material, which facilitates the rapid diffusion and conversion of electrolyte ions. Fig. 5 (b) shows the charge and discharge curves for different current densities. The shape of the charge and discharge curve is triangular at different current densities and all curves have good symmetry

at different current densities, which means that the material has good capacitance and electrochemical reversibility. Fig. 5(c) shows the impedance curve, which is said to show a relatively low equivalent series resistance (ESR) and a shorter Warburg region. Fig. 5(d) is a graph of energy density and power density. At a power density of 499.9 W kg-1, the energy density is 5.7 Wh kg^{-1}, while the energy density drops to 3.6 Wh kg^{-1} and the power density is 10000 W kg^{-1}.

To further evaluate the practical application of electrode materials immersed in absorbent cotton in $ZnCl_2$ and $Mg(NO_3)_2$, we assembled a symmetrical supercapacitor and tested it in a 1 M Na_2SO_4 aqueous solution. Fig. 6(a) is a cyclic voltammetry curve of an electrode material immersed in absorbent cotton in $ZnCl_2$ and $Mg(NO_3)_2$ at different potential windows at a scanning rate of 50 mV s^{-1}. When the potential window is low, the shape of the CV curve is close to a rectangle. When the voltage window is large, the capacitor current increases sharply and the CV curve is distorted. It is benefited from the decomposition of the electrolyte that the electrode material at high potential polarized [28, 42]. Fig. 6(b) shows the CV curves for the potential window at different scan rates at 0-1.6V. All CV curves exhibit an approximately rectangular shape at different scan rates. This means good rate performance and double layer capacitance. This result is caused by high specific surface area of the material, which facilitates the rapid diffusion and conversion of electrolyte ions. Fig. 6(c) is a charge and discharge curve of different current densities. The current charge and discharge curve shows a slightly deformed triangular shape at a low current density, and the current charge and discharge curve shows a slightly deformed triangular shape at a low current density, revealing EDLC and the coexistence of pseudocapacitive.

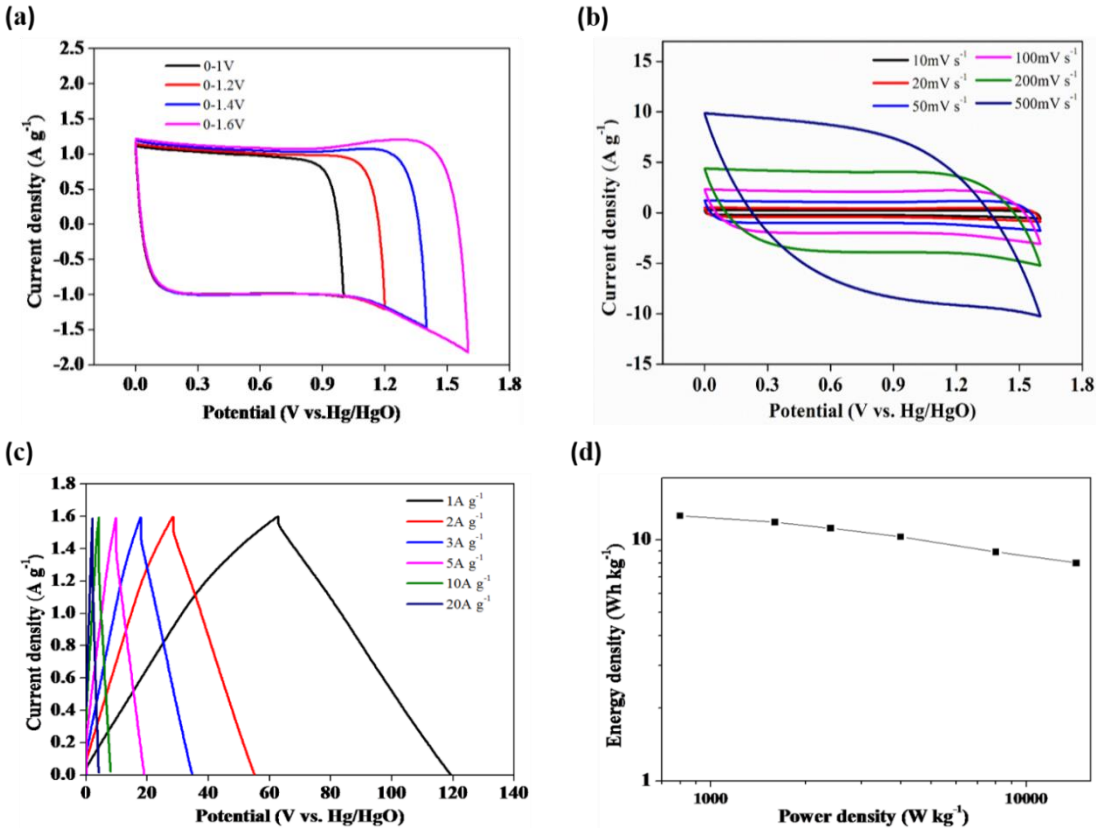

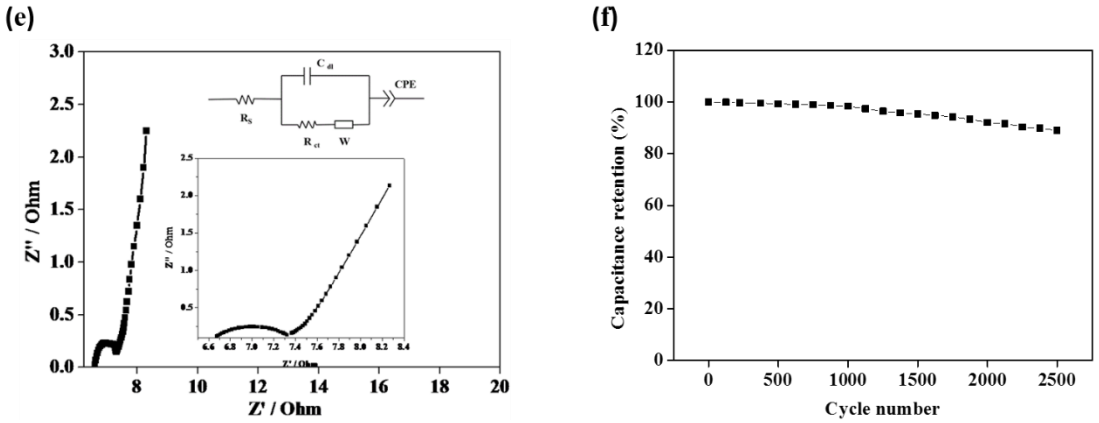

Figure 6. (a) Cyclic voltammetry curves for different potential windows for electrode materials impregnated in $ZnCl_2$ and $Mg(NO_3)_2$ at a scan rate of 50 mV s^{-1}; (b) CV curves of different scanning rates with a potential window of 1.6 V; (c)The charge and discharge curves at different current densities; (d) Curves of Energy density and Power density at current density of 1A g^{-1}, 2 A g^{-1}, 3A g^{-1}, 5A g^{-1}, 10A g^{-1}, 20A g^{-1}, respectively; (e) EIS curve; (f) Cyclic stability curve (scan rate is 200mV s^{-1} for 2500 cycles);

Fig. 6(d) is a plot of energy density versus power density with an energy density of 12.5 Wh kg^{-1} at a power density of 799.9 W kg^{-1} and an energy density of 8 Wh kg^{-1} with a power density of 14400 W kg^{-1}. Fig. 6(e) shows the Nyquist plot of the symmetric cell. The inset is the well-fitted equivalent circuit, which comprises the following several parts: Rs (the solution resistance), R_{ct} (the charge-transfer resistance), W (the Warburg impedance), C_{dl} (the double-layer capacitance) and CPE (the constant phase element) [43]. It can be shown that the internal resistance is low due to the small diameter of the semicircle in high frequency region, which can meet the demands of industrial application [44]. Fig. 6(f) shows a symmetrical supercapacitor exhibiting an initial capacitance retention of 89% in a cycle of 2500 cycles and a scan rate of 200 mV s^{-1}.

Table 2. Comparison of activating agent, specific surface area and specific capacitance of different materials

Carbon source	Activating agent	S_{BET} (m^2 g^{-1})	Specific capacitance (F g^{-1})	Electrolyte	Ref
Absorbent cotton	$ZnCl_2$	1900	240	6 M KOH	This work
cotton stalk	KOH	1877	180	1 M Et4NBF4/AN	45
cotton fibers	NaOH	584	198	6 M KOH	46
cotton stalk	H_3PO_4	1481	114	1 M Et_4NBF_4	47
Cow dung	KOH	1984	117	1 M Et_4NBF_4	48
Peanut shell	$ZnCl_2$	1552	184	6 M KOH	49
Rice husk	H_3PO_4	1490	112	1 M Na_2SO_4	50
Yogurt	KOH	1300	225	1 M H_2SO_4	51
Willow leaves	$ZnCl_2$	1031	216	6 M KOH	52
Firewood	Na_2CO_3 K_2CO_3	818	189	1 M H_2SO_4	53

Table 2 uses biomass as a raw material to prepare a biomass-based porous carbon material, wherein the experiment and 45, 46, and 47 carbon materials prepared by using cotton as a raw material under different activator conditions. Compared with other materials, it can be seen that the specific surface area and specific capacitance of the carbon material prepared by using $ZnCl_2$ as an activator are larger. In addition, this work and 49, 52 biomass-based porous carbon materials prepared by using $ZnCl_2$ as an activator for different biomass materials, carbon materials prepared from absorbent cotton as compared to other materials have a larger specific surface area and specific capacitance.

4. CONCLUSION

A porous carbon material was prepared using cotton as a raw material $ZnCl_2$ as an activator and MgO as a template. The material as an electrode material has a specific capacitance of 240 F g^{-1} at a current density of 1 A g^{-1} in a three-electrode system, and a capacitance retention of 71%. In addition, a symmetric electrode supercapacitor is assembled from the material. The maximum energy density of the current density of 1 A g^{-1} under alkaline electrolyte is 5.7 Wh kg^{-1}. The maximum energy density at a current density of 1 A g^{-1} under a neutral electrolyte was 12.5 Wh kg^{-1}, and the cycle stability was 89%. The reason is mainly due to the interconnected porous structure, high surface area (1990 m^2 g^{-1}), which will promote rapid charge transfer, rapid charge and discharge. Therefore, this material is promising for the synthesis of low cost and sustainable supercapacitor electrode materials.

References

1. A. Kaneko, Y. Hayashi And S. Nonaka, *Electr Eng Jpn.*, 205 (2018) 3.
2. C. Long, L. Jiang, X. Wu, Y. Jiang, D. Yang, C. Wang, T. Wei And Z. Fan, *Carbon*, 93 **(**2015) 412.
3. L. Jiang, L. Sheng And Z. Fan, *Sci China Mater.*, 61 **(**2018), 133.
4. J. Guo And P. Zheng, *Mater Lett.*, 214 **(**2017) 134.
5. P. Liu, Y. Zhu, X. Gao, Y. Huang, Y. Wang, S. Qin And Y. Zhang, *Chem Eng J.*, 350 **(**2018) 79.
6. C. Han, Y. Ye, G. Wang, W. Hong And C. Feng, *Chem Eng J.*, 347 **(**2018) 648.
7. D. Momodu, A. Bello, K. Oyedotun, F. Ochai-Ejeh, J. Dangbegnon, M. Madito And N. Manyala, *Rsc Adv.*, 7 **(**2017) 37286.
8. Y. Wei, *Chem Lett.*, 43 **(**2014) 216.
9. Z. Ye, F. Wang, C. Jia And Z. Shao, *J Mater Sci.*, 53 **(**2018) 12374.
10. P. Song, X. Shen, W. He, L. Kong, X. He, Z. Ji, A. Yuan, G. Zhu And N. Li, *J Mater Sci-Mater El.*, 29 **(**2018) 12206.
11. X. Zhao, H. Chen, S. Wang, Q. Wu, N. Xia And F. Kong, *Mater Chem Phys.*, 215 **(**2018) 157.
12. N. I. T. Ramli, S. Abdul Rashid, Y. Sulaiman, M. S. Mamat, S. A. Mohd Zobir And S. Krishnan, *J Power Sources.*, 328 **(**2016) 195.
13. X. Su, S. Jiang, G. Zheng, X. Zheng, J. Yang And Z. Liu, *J Mater Sci.*, 53 **(**2018) 9191.
14. H. Seifi And S. Masoum, *Int J Hydrogen Energ.*, 42 **(**2017) 30145.
15. Y. Yao, Q. Zhang, P. Liu, L. Yu, L. Huang, S. Zeng, L. Liu, X. Zeng And J. Zou, *Rsc Adv.*, 8 **(**2018) 1857.
16. D. Puthusseri, V. Aravindan, B. Anothumakkool, S. Kurungot, S. Madhavi And S. Ogale, *Small*, 10

(2014) 4395.
17. S. Yan, J. Lin, P. Liu, Z. Zhao, J. Lian, W. Chang, L. Yao, Y. Liu, H. Lin And S. Han, *Rsc Adv.*, 8 **(**2018) 6806.
18. Q. Tian, X. Wang, X. Xu, M. Zhang, L. Wang, X. Zhao, Z. An, H. Yao And J. Gao, *Mater Chem Phys.*, 213 **(**2018) 267.
19. C. Long, X. Chen, L. Jiang, L. Zhi And Z. Fan, *Nano Energy*, 12 (2015) 141.
20. X. Su, S. Li, S. Jiang, Z. Peng, X. Guan And X. Zheng, *Adv Powder Technol.*, 29 (2018) 2097.
21. H. Souri And D. Bhattacharyya, *Acs Appl Mater Inter.*, 10 (2018) 20845.
22. B. Saravanakumar, S. Muthulakshmi, G. Ravi, V. Ganesh, A. Sakunthala And R. Yuvakkumar, *Appl Phys A.*, 123 (2017).
23. B. Wang, Y. Wang, Y. Peng, X. Wang, N. Wang, J. Wang And J. Zhao, *Chem Eng J.*, 348 (2018) 850.
24. L. Zhang, L. Xu, Y. Zhang, X. Zhou, L. Zhang, A. Yasin, L. Wang And K. Zhi, *Rsc Adv.*, 8 (2018) 3869.
25. J. Cao, C. Zhu, Y. Aoki And H. Habazaki, *Acs Sustain Chem Eng.*, 6 (2018) 7292.
26. H. Qu, X. Zhang, J. Zhan, W. Sun, Z. Si And H. Chen, *Acs Sustain Chem Eng.*, 6 (2018) 7380.
27. C. Zhu And T. Akiyama, *Green Chem.*, 18 (2016) 2106.
28. H. Chen, H. Wei, N. Fu, W. Qian, Y. Liu, H. Lin And S. Han, *J Mater Sci.*, 53 (2018) 2669.
29. Q. Yao, H. Wang, C. Wang, C. Jin And Q. Sun, *Acs Sustain Chem Eng.*, 2018, **6**, 4695-4704.
30. D. Zeng, Y. Dou, M. Li, M. Zhou, H. Li, K. Jiang, F. Yang And J. Peng, *J Mater Sci.*, 53 (2018) 8372.
31. Y. Shi, L. Zhang, T. B. Schon, H. Li, C. Fan, X. Li, H. Wang, X. Wu, H. Xie, H. Sun, D. S. Seferos And J. Zhang, *Acs Appl Mater Inter.*, 9 (2017) 42699.
32. Y. Zhang, H. Jiang, Q. Wang, J. Zheng And C. Meng, *Appl Surf Sci.*, 447 (2018) 876.
33. Z. Liu, Z. Zhu, J. Dai And Y. Yan, *Chemistryselect.*, 3 (2018) 5726.
34. G. Zhang, Y. Chen, Y. Chen And H. Guo, *Mater Res Bull.*, 102 (2018) 391.
35. J. Pang, W. Zhang, H. Zhang, J. Zhang, H. Zhang, G. Cao, M. Han And Y. Yang, *Carbon.*, 132 (2018) 280.
36. J. Wei, S. Wan, P. Zhang, H. Ding, X. Chen, H. Xiong, S. Gao And X. Wei, *New J Chem.*, 42 (2018) 6763.
37. G. Fu, Q. Li, J. Ye, J. Han, J. Wang, L. Zhai And Y. Zhu, *J Mater Sci-Mater El.*, 29 (2018) 7707.
38. W. Kang, B. Lin, G. Huang, C. Zhang, Y. Yao, W. Hou, B. Xu And B. Xing, *J Mater Sci-Mater El.*, 29 (2018) 6361.
39. T. Liu, B. Lee, M. J. Lee, J. Park, Z. Chen, S. Noda And S. W. Lee, *J Mater Chem A.*, 6 (2018) 1.
40. X. Zhang, Q. Niu, Y. Guo, X. Gao And K. Gao, *Rsc Adv.*, 8 (2018) 16433.
41. G. Lin, F. Wang, Y. Wang, H. Xuan, R. Yao, Z. Hong And X. Dong, *J Electroanal Chem.*, 758 (2015) 39.
42. L. Jiang, L. Sheng, X. Chen, T. Wei And Z. Fan, *J Mater Chem A.*, 4 (2016) 11388.
43. Y. Wang, H. Xuan, G. Lin, F. Wang, Z. Chen And X. Dong, *J Power Sources.*, 319 (2016) 262.
44. M. Chen, H. Xuan, X. Zheng, J. Liu, X. Dong And F. Xi, *Electrochim Acta*, 238 (2017) 269.
45. W. Li, T. Wumaier, M. Chen, J. Zhang, H. Liu, L. Yang and H. Wang, *J Solid State Electr.,* 20 (2016), 2315.
46. Y. Liu, Z. Shi, Y. Gao, W. An, Z. Cao, and J. Liu, *ACS APPL Mater Inter*., 8 (2016) 28283.
47. M. Chen, X. Kang, T. Wumaier, J. Dou, B. Gao, Y. Han, G. Xu, Z. Liu, and L. Zhang, *J Solid State Electr*., 17 (2013), 1005.
48. D. Bhattacharjya And J. Yu, *J Power Sources*, 262 (2014) 224.
49. X. He, R. Li, J. Han, M. Yu And M. Wu, *Mater Lett.*, 94 (2013), 158.
50. A. Ganesan, R. Mukherjee, J. Raj And M. M. Shaijumon, *J Porous Mat.*, 21 (2014) 839.
51. M. Wahid, G. Parte, D. Phase And S. Ogale, *J Mater Chem A.*, 3 (2015) 1208.
52. Y. Liu, Y. Wang, G. Zhang, W. Liu, D. Wang And Y. Dong, *Mater Lett.*, 176 (2016) 60.

53. B. Lu, L. Hu, H. Yin, W. Xiao And D. Wang, *Rsc Adv.*, 6 (2016) 106485.